Ma et al. *Zool. Res.* 2026, 47(3): 913−928
https://doi.org/10.24272/j.issn.2095-8137.2025.302
https://cstr.cn/32248.14.zr.2025.302

ZR | Zoological Research

Article Open Access

Single-cell RNA sequencing reveals IgM$^+$ B cell differentiation and protective responses after DNA vaccination and *Vibrio anguillarum* challenge in flounder (*Paralichthys olivaceus*)

Zhen-Jie Ma[1], Hong-Fei Tian[1], Jing Xing[1,2,*], Xiao-Qian Tang[1], Xiu-Zhen Sheng[1], Heng Chi[1], Wen-Bin Zhan[1,2]

[1] *Laboratory of Pathology and Immunology of Aquatic Animals*, *KLMME*, *Shandong Key Laboratory of Green Mariculture and Smart Fisheries*, *Ocean University of China*, *Qingdao* 266003, *China*

[2] *Laboratory for Marine Fisheries Science and Food Production Processes*, *Qingdao Marine Science and Technology Center*, *Qingdao*, *Shandong* 266237, *China*

ABSTRACT

B cells are central mediators of vaccine-induced protective immunity in vertebrates. However, cellular programs through which teleost B cells contribute to vaccine-mediated protection remain poorly elucidated. To assess these responses, flounder were intramuscularly immunized with a *Vibrio anguillarum* DNA vaccine and challenged 35 days after immunization. Head kidney IgM$^+$ B cells were isolated using a previously established monoclonal antibody and subjected to single-cell RNA sequencing at 7 days post-challenge. Seven IgM$^+$ B cell subsets were resolved: innate B cells, CXCR4$^+$ B cells, mature B cells, plasmablasts, TIRAP$^+$ B cells, CD22$^+$ B cells, and CD44$^+$ B cells. Trajectory reconstruction identified three differentiation routes, with CXCR4$^+$ B cells and mature B cells representing transitional states closely linked to B cell-mediated protective immunity. Innate B cells and plasmablasts showed prominent enrichment of phagocytic and antibody-secretion programs, respectively. Vaccination expanded both CXCR4$^+$ and mature B cell subsets and enhanced pathways associated with T cell interactions, indicating increased capacity to coordinate T cell-dependent immune responses. Plasmablasts also underwent a transcriptional shift from effector activation toward immune homeostasis, suggesting a sustained contribution to long-term protection. These findings demonstrate the functional heterogeneity and differentiation architecture of teleost IgM$^+$ B cells and identify T cell-associated B cell subsets as critical cellular mediators of DNA vaccine-induced protection. This study provides new insight into B cell differentiation and vaccine-responsive adaptive immunity in teleosts and broadens understanding of conserved and lineage-specific mechanisms of vertebrate adaptive immunity.

Keywords: *Paralichthys olivaceus*; IgM$^+$ B cells; Vaccination; Single-cell RNA sequencing; Differentiation trajectory

INTRODUCTION

B cells are fundamental effectors of vaccine-induced protection in vertebrates, primarily through antibody secretion and the establishment of durable humoral immunity. In mammals, B cell development occurs in the bone marrow, followed by germinal center entry, somatic hypermutation, affinity maturation, and differentiation into high-affinity antibody-secreting cells and long-lived memory populations. These processes have provided a conceptual and mechanistic foundation for modern vaccine design, including SARS-CoV-2 vaccines (Lapuente et al., 2024). In contrast, teleost B cell immunity operates within a markedly different anatomical and evolutionary framework. Teleosts lack bone marrow and lymph nodes, as well as the highly organized lymphoid architectures that support mammalian adaptive immune responses (Fänge, 1986). Consequently, hematopoiesis, lymphocyte generation, and immune cell enrichment occur primarily in the kidney, particularly the head kidney, which represents a central immune organ in teleosts (Bromage et al., 2004; Zwollo et al., 2005). Significant differences between teleosts and mammals also extend to immunoglobulin (Ig) composition. Based on immunoglobulin heavy-chain isotypes, teleost antibodies comprise IgM, IgD, and IgT/Z, a mucosa-associated immunoglobulin class unique to teleosts (Sun et al., 2020). Among these isotypes, IgM constitutes the dominant mediator of systemic humoral immunity in peripheral blood and remains the most extensively characterized

Received: 04 September 2025; Accepted: 08 December 2025; Online: 09 December 2025

Foundation items: This study was supported by the National Key Research and Development Program of China (2023YFD2400702, 2018YFD0900503), National Natural Science Foundation of China (32173005), and Fundamental Research Funds for the Central Universities (202561039)

*Corresponding author, E-mail: xingjing@ouc.edu.cn

antibody class in teleost immunology (Bromage et al., 2004). Beyond antibody secretion, teleost B cells also retain a prominent innate-like functional repertoire. Compared with mammalian B cells, teleost B cells exhibit substantially higher phagocytic capacity, including increased phagocytic percentages and indices (Li et al., 2006; Rabinovitch, 1995). This phagocytic activity is mediated by multiple surface receptors, including pattern-recognition receptors such as Toll-like receptors (TLRs), Fc receptors, and complement receptors, which recognize pathogen-associated molecular patterns or opsonized pathogens to initiate phagocytosis (Boshra et al., 2005; Hao et al., 2024; Soleto et al., 2020). Through this dual capacity for antibody production and direct pathogen uptake, teleost B cells integrate adaptive and innate immune functions, providing a versatile defense strategy suited to the distinct organization of the teleost immune system (Wu et al., 2020).

In teleosts, B cells play a crucial role in vaccine-induced immunity (Rauta et al., 2012). Upon antigen exposure, membrane-bound immunoglobulin (mIg) enables B cells to recognize cognate epitopes, internalize antigen, and present processed peptides through MHC II molecules. Recognition of peptide-MHC II complexes by helper T cells provides costimulatory signals that support B cell clonal expansion and differentiation into antibody-secreting plasma cells (Ma et al., 2019; Rathor & Swain, 2024). Plasma cells subsequently produce antigen-specific antibodies, whereas memory B cells retain antigen-recognition receptors that support accelerated humoral responses upon re-exposure to the same antigen (Bromage et al., 2004). Within this immune framework, the head kidney plays a vital role as the primary site of B cell development and proliferation, functionally resembling mammalian bone marrow (Zwollo et al., 2005). In rainbow trout (*Oncorhynchus mykiss*), bacterial antigen exposure induces immune cell aggregation within melanomacrophage centers (MMCs) in the head kidney (Shibasaki et al., 2023). Although teleosts lack conventional germinal centers, MMCs exhibit selected structural and functional parallels with mammalian germinal centers and have been proposed as potential sites contributing to adaptive immune responses (Steinel & Bolnick, 2017). After vaccination, head kidney IgM^+ B cells mount robust IgM responses that contribute to systemic protection (Ye et al., 2011). These cells also show pronounced phagocytic activity, indicating that head kidney B cells participate in vaccine-mediated protection through both antibody-dependent immunity and direct pathogen clearance (Munang'andu & Evensen, 2019).

Despite considerable progress in teleost immunology, the protective functions and differentiation programs of vaccine-responsive B cell subsets remain insufficiently defined. Recent advances in single-cell RNA sequencing (scRNA-seq) provide a high-resolution framework for resolving immune cell heterogeneity, lineage dynamics, and activation states at the single-cell level, thereby enabling a deeper characterization of teleost B cell differentiation during vaccine-induced immune responses (Chan et al., 2022; Villani et al., 2017). Previous studies have shown that the VAA recombinant protein from *Vibrio anguillarum* can significantly induce humoral immunity in flounder (*Paralichthys olivaceus*), leading to the development of a DNA vaccine candidate encoding VAA (pVAA) (Xing et al., 2017, 2019). After intramuscular pVAA immunization, antibody titers and the proportion of IgM^+ B cells peaked at 35 days, and subsequent challenge with *V. anguillarum* produced a 50% relative protection rate in the pVAA group compared with the control group, with mortality restricted to the first 7 days after challenge (Xing et al., 2019).

In the present study, a flounder vaccine-response model was established through intramuscular administration of pVAA, followed by *V. anguillarum* challenge after a 35-day primary immunization period. At 7 days post-challenge, IgM^+ B cells were isolated from the head kidney and analyzed by scRNA-seq to define the cellular architecture and transcriptional responses of vaccine-responsive B cell populations. This approach enabled systematic characterization of distinct IgM^+ B cell subsets and their contributions to innate and adaptive immune protection. Resolving the functional specialization and differentiation trajectories of head kidney IgM^+ B cells after vaccination and bacterial challenge advances our understanding of teleost B cell immunity and provides a cellular framework for the rational development of more effective vaccines for aquaculture.

MATERIALS AND METHODS

Ethics statement

All animal procedures adopted in this study were approved by the Animal Care and Use Steering Committee of Ocean University of China (permit number: OUC-AE-2025-019). Every possible effort was made to minimize animal suffering.

Fish, bacteria, DNA vaccine plasmid, and antibody

Healthy flounder (6 months old, 22±3 cm long, 120±20 g) were purchased from a mariculture farm in Rizhao, Shandong Province, China. Fish were randomly allocated to six 200 L plastic tanks (three tanks/group) and maintained in recirculating seawater at 21±1℃. Fish were fed sinking commercial pellets (Bessn Co., Shandong, China) twice daily and acclimated for 1 week before experimentation. Throughout the experiment, water was maintained at 21±1℃, with dissolved oxygen of 7.5–8.5 mg/L, salinity of 32±1 ppt, and pH of 7.8–8.2.

The pathogenic strain *Vibrio anguillarum* SJ060621 was maintained at the Laboratory of Pathology and Immunology of Aquatic Animals (LPIAA), Ocean University of China, Qingdao, Shandong, China (Tang et al., 2008). The strain was cultured in 2216E marine broth, prepared at LPIAA according to the Difco™ 2216E formulation (BD Biosciences, Sparks, MD, USA), at 28℃ for 24 h. Bacterial cells were collected by centrifugation at 8 000×*g* for 10 min at 4℃, washed twice with sterile phosphate-buffered saline (PBS), and resuspended in PBS. Bacterial concentration was determined using the volume-based counting function of an Accuri C6 cytometer (BD Biosciences, Piscataway, NJ, USA). A suspension of *V. anguillarum* at 1.0×10^7 CFU/mL was prepared for challenge experiments.

The *V. anguillarum* DNA vaccine plasmid pVAA was previously constructed and stored at LPIAA (Xing et al., 2019). Briefly, pVAA was generated using the eukaryotic expression vector pcDNA3.1 and the full-length VAA gene (GenBank accession number: WP_013857004.1), which encodes an adhesion antigen from *V. anguillarum* previously shown to confer 78.38% relative percent survival (RPS) upon recombinant protein immunization (Xing et al., 2017). Plasmid DNA was extracted using an EndoFree Plasmid Kit (Tiangen, Beijing, China), and the concentration was adjusted to 200 ng/μL using a NanoDrop 8000 spectrophotometer (Thermo Fisher Scientific, Waltham, MA, USA). The plasmid was stored at −20℃ until use.

A mouse anti-flounder IgM monoclonal antibody previously generated and stored at LPIAA (Li et al., 2007) was used for IgM^+ cell sorting in subsequent experiments.

Vaccination and challenge

A total of 200 fish were randomly assigned to a vaccine group administered pVAA and a control group administered pcDNA3.1 (100 fish/group). After 1 week of acclimation, 20 μg of pVAA or pcDNA3.1 was injected intramuscularly into the epaxial muscle below the dorsal fin. On day 35 post-vaccination, fish were challenged by intraperitoneal injection with live *V. anguillarum* (1.0×10^6 CFU/fish). Mortality was recorded separately for each group throughout the challenge period. On day 7 post-challenge, nine fish from each group were randomly selected, anesthetized, and euthanized with MS-222 (Sigma, Saint Louis, MO, USA). Blood was collected from the caudal vein using a heparinized needle, and the head kidney was aseptically dissected for leukocyte isolation and subsequent sorting of IgM^+ B cells.

Cell sorting by flow cytometry

Head kidney tissues collected after vaccination and bacterial challenge were processed for leukocyte isolation by Percoll density gradient centrifugation, as described previously (Tian et al., 2021). In brief, head kidney tissues were excised aseptically, and single-cell suspensions were generated by gently pressing the tissues through nylon gauze in 65% RPMI-1640 medium. Cell suspensions were centrifuged at 100×g for 10 min at 4℃ and the resulting pellets were layered onto a discontinuous Percoll density gradient (1.020–1.070 g/cm^3). Following further centrifugation at 840×*g* for 30 min at 4℃, lymphocyte layers at the Percoll interface were carefully collected. Cell suspensions were then adjusted to 1×10^7 cells/mL and maintained on ice until further processing. To detect IgM^+ cells in the flounder head kidney, leukocytes were incubated with mouse anti-flounder IgM monoclonal antibody (MAb; 1:1 000), followed by Alexa Fluor 488-conjugated goat anti-mouse IgG secondary antibody (1:1 000; Thermo Fisher Scientific, Waltham, MA, USA). IgM^+ cells were then sorted and assayed using a BD FACSAria™ Fusion Flow Cytometer (BD Biosciences), assessed for viability, and processed for scRNA-seq, as reported previously (Tian et al., 2021).

Immunofluorescence microscopy

Cell morphology before and after sorting was evaluated using smears prepared from head kidney lymphocyte suspensions and flow cytometry-sorted IgM^+ cell suspensions, respectively. In brief, cell suspensions were collected and fixed in 4% paraformaldehyde at room temperature for 15 min. Cells were then blocked with 5% bovine serum albumin (BSA) for 1 h and incubated with mouse anti-flounder IgM monoclonal antibody (1:1 000; produced and stored at LPIAA) for 1.5 h at 37℃. For negative controls, purified serum from unimmunized mice was used in place of the primary antibody. After washing three times with PBST, cells were incubated with Alexa Fluor 488-conjugated goat anti-mouse IgG secondary antibody (1:1 000; Thermo Fisher Scientific, Waltham, MA, USA) at room temperature for 45 min. Nuclei were subsequently counterstained with 4',6-diamidino-2-phenylindole (DAPI, BioLegend) in the dark. Fluorescence images were captured using a fluorescence microscope (LSM900 with Airyscan 2, ZEISS, Germany).

ScRNA-seq of flounder IgM^+ cells

ScRNA-seq was performed after verifying cell viability exceeded 90% and adjusting the live-cell concentration to 1 000–2 000 cells/μL. In brief, IgM^+ cells were processed using the 10× Genomics Chromium Next GEM Single Cell 3' Reagent Kit v.3.1 to generate Gel Beads in Emulsion (GEMs). Upon gel bead dissolution, primers containing an Illumina R1 sequence, a 16 nt cell-specific barcode, a 10 nt unique molecular identifier (UMI), and a poly(dT) sequence were released, enabling barcoding of polyadenylated mRNA from individual cells during reverse transcription. Standard sequencing libraries were subsequently amplified using polymerase chain reaction (PCR), and libraries from the control and vaccine groups were subjected to high-throughput sequencing on the Illumina platform using PE150 sequencing mode (10× Genomics) (Satija et al., 2015).

Single-cell RNA-seq data processing

Raw single-cell sequencing data were processed using Cell Ranger from 10× Genomics for quality control, read alignment, gene-expression quantification, and generation of a gene-cell expression matrix (http://software.10xgenomics.com/single-cell/overview/welcome). After gene-expression matrices were generated, downstream clustering, cell subset annotation, and differentially expressed gene (DEG) analysis were performed using Seurat (https://satijalab.org/seurat/) (Qiu et al., 2017a). Reads were aligned to the *Paralichthys olivaceus* reference genome NC_002386.1 (GenBank: AB028664.1) (https://www.ncbi.nlm.nih.gov/). Harmony was then applied to reduce batch-associated variation and condition-associated effects before clustering (Korsunsky et al., 2019). Cell clusters were identified using the Louvain algorithm at a resolution of 0.7. To preserve relationships among transcriptionally related cell populations, single-cell transcriptomes were visualized by Uniform Manifold Approximation and Projection (UMAP) for dimensionality reduction (Becht et al., 2019).

Pseudotime trajectory analysis

Because preliminary trajectory inference with Monocle 2 did not clearly resolve differentiation pathways among flounder IgM^+ B cells, RNA velocity, Partition-based Graph Abstraction (PAGA), and Slingshot were integrated to obtain a more accurate characterization of cellular transitions. RNA velocity analysis was performed using velocyto v.0.17.17, which uses relative abundances of unspliced and spliced mRNA as an indicator of future cell state (La Manno et al., 2018). Spliced and unspliced reads were annotated from BAM files using velocyto with default parameters. RNA velocity vectors were projected onto the UMAP embedding, with vector direction and magnitude indicating the predicted direction and rate of cell-state transition. Directional flow across the velocity field was used to infer hierarchical relationships among cell populations.

PAGA was then applied to define graph-based connectivity among cell subsets and infer transitions between transcriptional states on the basis of RNA velocity results (Wolf et al., 2019). Because PAGA integrates cluster-level topology with transition structure, it provided a complementary framework for resolving relationships among IgM+ B cell subsets.

Slingshot was subsequently used after dimensionality reduction and clustering to infer developmental trajectories in the flounder IgM^+ cell dataset. Based on RNA velocity and PAGA results, innate B cells were selected as a starting population for Slingshot trajectory reconstruction using the R package Slingshot (Street et al., 2018).

Up-regulated gene analysis

Subset-enriched marker genes were identified using the

Wilcoxon rank-sum test by comparing gene expression in each subset with expression in all remaining cells (Camp et al., 2017). Up-regulated genes were defined using the following criteria: expression at least 1.28-fold higher in the target cluster ($log_2FC \geq 0.36$), detection in more than 25% of cells within the target population, and $P<0.05$. Up-regulated genes from each subset were subjected to Gene Ontology (GO) and Kyoto Encyclopedia of Genes and Genomes (KEGG) enrichment analyses. GO analysis included functional classification and significance enrichment of proteins encoded by up-regulated genes. These proteins were mapped to terms in the GO database (http://www.geneontology.org/) and GO terms with $P<0.05$ were considered significantly enriched (Ashburner et al., 2000). KEGG (http://www.genome.ad.jp/kegg/) is the main public database on pathways, applying a hypergeometric test to identify pathways significantly enriched in up-regulated expressed proteins compared to background proteins in terms of KEGG pathway (Kanehisa & Goto, 2000). Pathways with $P<0.05$ were selected to be defined as pathways significantly enriched in up-regulated expressed proteins. Similarly, the same approach as described above was used in determining the genetic and functional differences between the two selected subsets. The same analytical strategy was used to define genetic and functional differences between the two selected subsets. Up-regulated genes assigned to enriched KEGG pathways in each subset were then mapped to the STRING database (https://string-db.org/), and interaction pairs with confidence scores >700 were retained for PPI network construction. Networks were visualized using Cytoscape v.3.8.2 (https://cytoscape.org/release_notes_3_8_2.html), with node size indicating connectivity. Duplicate gene symbols were labeled using gene ID+symbol.

Differentially expressed gene analysis

To identify genes and signaling pathways that differed between the vaccine and control groups within each cluster, cluster-specific DEGs were identified using the Wilcoxon rank-sum test. DEGs were screened using fold change≥1.28, $P<0.05$, and expression in more than 25% of cells in at least one comparison group. DEGs from each cluster were then subjected to GO and KEGG enrichment analyses using a threshold of $P<0.05$. GO terms and KEGG pathways meeting this criterion were considered significantly enriched among DEGs.

Statistical analysis

Differences in IgM^+ cells between two groups were analyzed using the FindMarkers function in Seurat, which applies the Wilcoxon rank-sum test by default. For comparisons among more than two groups, statistical significance was determined by one-way analysis of variance (ANOVA) followed by Tukey's *post hoc* test. Statistical analyses and figure generation were performed using GraphPad Prism (GraphPad Software), R (R Project for Statistical Computing), Omicsmart, and BioRender.

RESULTS

Proportion of sorted IgM^+ cells and quality control of scRNA-seq data

Head kidney IgM^+ B cells were isolated from flounder immunized with the *V. anguillarum* DNA vaccine and profiled by scRNA-seq to define vaccine-responsive B cell states (Figure 1A). The structural and molecular characteristics of the VAA protein are shown in Supplementary Figure S1, S2 and Supplementary Table S1. Survival was monitored throughout the 45 day experimental period (Supplementary Figure S3). Flow cytometry confirmed the proportion of sorted IgM^+ cells, and immunofluorescence microscopy showed the cellular morphology of the sorted IgM^+ population (Figure 1B, D). After quality assessment confirmed that sorted IgM^+ B cells met the requirements for scRNA-seq, cell suspensions were adjusted to 700–1 200 cells/μL and processed using the 10× Genomics platform. Following quality control, gene and unique molecular identifier (UMI) distributions were assessed (Supplementary Figure S4), and 2 179 and 3 644 IgM^+ cells were retained from the vaccine and control groups, respectively.

ScRNA-seq-identified IgM^+ B cell subsets in the head kidney

Unsupervised clustering of head kidney IgM^+ cells resolved seven transcriptionally distinct subsets, which were visualized by UMAP (Figure 1C). CD79a (Igα) and CD79b (Igβ), invariant components of the B cell receptor (BCR) complex that are highly conserved in teleosts, were used as canonical markers to confirm B cell identity (Dornburg & Yoder, 2022). Robust expression of these markers in the sorted IgM^+ population verified successful enrichment of B cells (Figure 1E). Based on the 30 marker genes and established functional features of flounder IgM^+ B cells, including antibody secretion, antigen presentation, and phagocytosis, the seven subsets were annotated as $TIRAP^+$ B cells, mature B cells, innate B cells, $CXCR4^+$ B cells, $CD22^+$ B cells, plasmablasts, and $CD44^+$ B cells (Hao et al., 2024; Sheng et al., 2019; Xing et al., 2018). Subset-enriched signature genes were visualized, highlighting the transcriptional features that distinguished each IgM^+ B cell population (Figure 1F).

Pseudotime analysis of IgM^+ cell development by PAGA, RNA velocity, and Slingshot

To reconstruct developmental relationships among flounder IgM^+ B cell subsets, pseudotime analyses were conducted using RNA velocity, PAGA, and Slingshot approaches. RNA velocity positioned a high proportion of innate B cells near an early transcriptional state, whereas most plasmablasts occupied terminal transcriptional states (Figure 2A). PAGA was then used to integrate pseudotime ordering with cluster identity and to represent intercluster relationships as a simplified topology based on transcriptional similarity (Figure 2B–D). Consistent with the RNA velocity results, PAGA identified innate B cells as the origin of differentiation and plasmablasts as the terminal state. Slingshot analysis further resolved three major developmental trajectories: lineage 1 (innate B cells–$TIRAP^+$ B cells–$CD22^+$ B cells–plasmablasts), lineage 2 (innate B cells–$CXCR4^+$ B cells–mature B cells–plasmablasts), and lineage 3 (innate B cells–$CXCR4^+$ B cells–$CD44^+$ B cells) (Figure 2E–H). These trajectories indicated two principal branch points: an early bifurcation between $TIRAP^+$ B cells and $CXCR4^+$ B cells and a later divergence between mature B cells and $CD44^+$ B cells.

Differences among key subsets involved in IgM^+ cell differentiation

To further define transcriptional and functional distinctions at the major trajectory branch points, differential gene expression analysis and KEGG pathway enrichment were performed between $TIRAP^+$ B cells and $CXCR4^+$ B cells and between mature B cells and $CD44^+$ B cells. $CXCR4^+$ B cells contained more up-regulated genes than $TIRAP^+$ B cells (Figure 3A) and showed enrichment across a broader set of immune-related

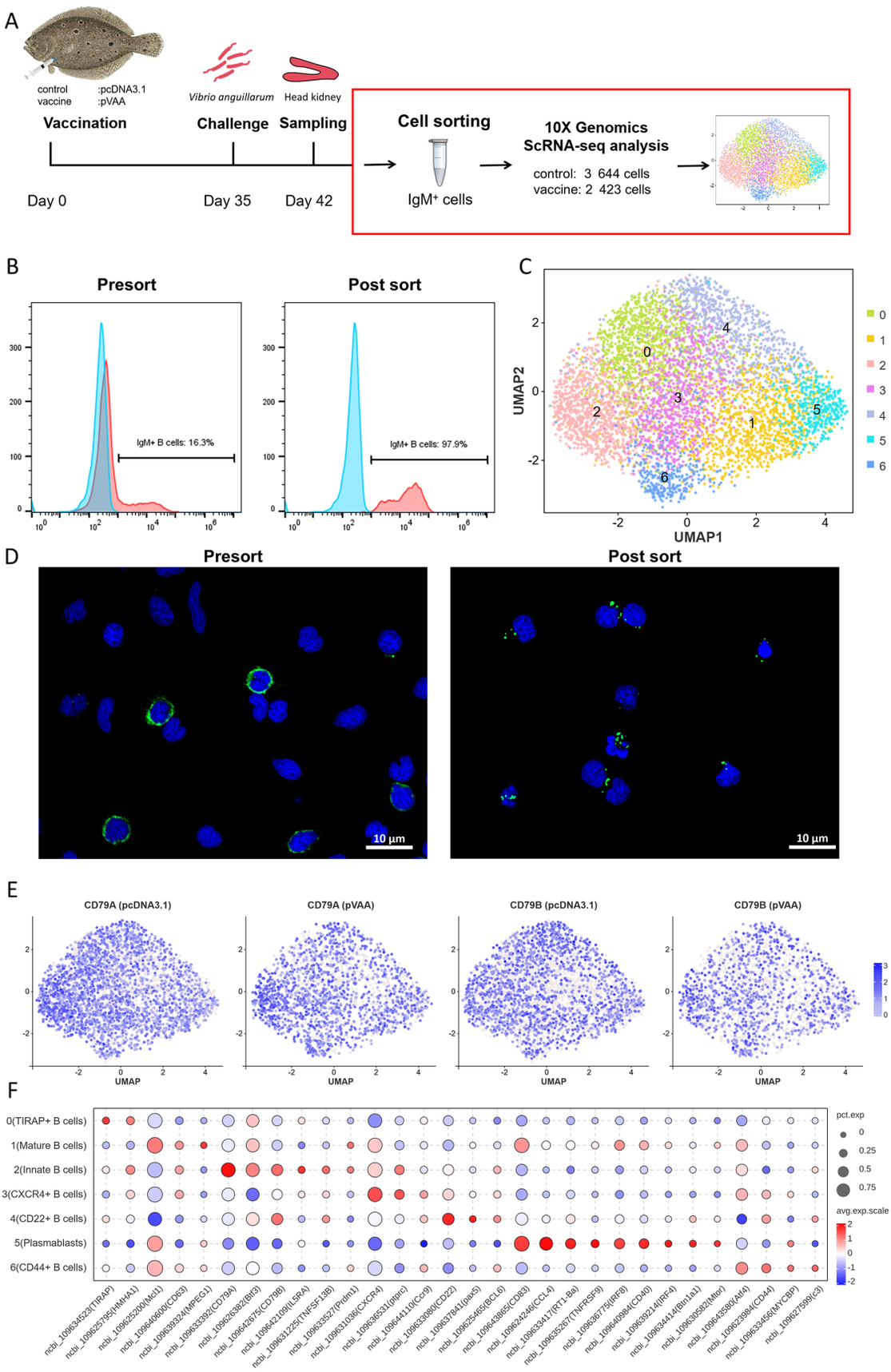

Figure 1 Single-cell transcriptomic atlas of IgM$^+$ B cell subsets in flounder after immunization

A: Experimental workflow showing vaccination, bacterial challenge, head kidney sampling, IgM$^+$ B cell sorting, and scRNA-seq analysis. B: Histogram showing proportion of IgM$^+$ B cells after cell sorting. C: UMAP visualization of head kidney IgM$^+$ B cells from control and vaccine groups, with colors denoting distinct IgM$^+$ B cell subsets. D: Immunofluorescence images showing head kidney IgM$^+$ cells before and after sorting. E: UMAP feature plots showing *CD79a* and *CD79b* expression in control and vaccine groups. F: Bubble plot showing selected marker gene expression across IgM$^+$ B cell subsets.

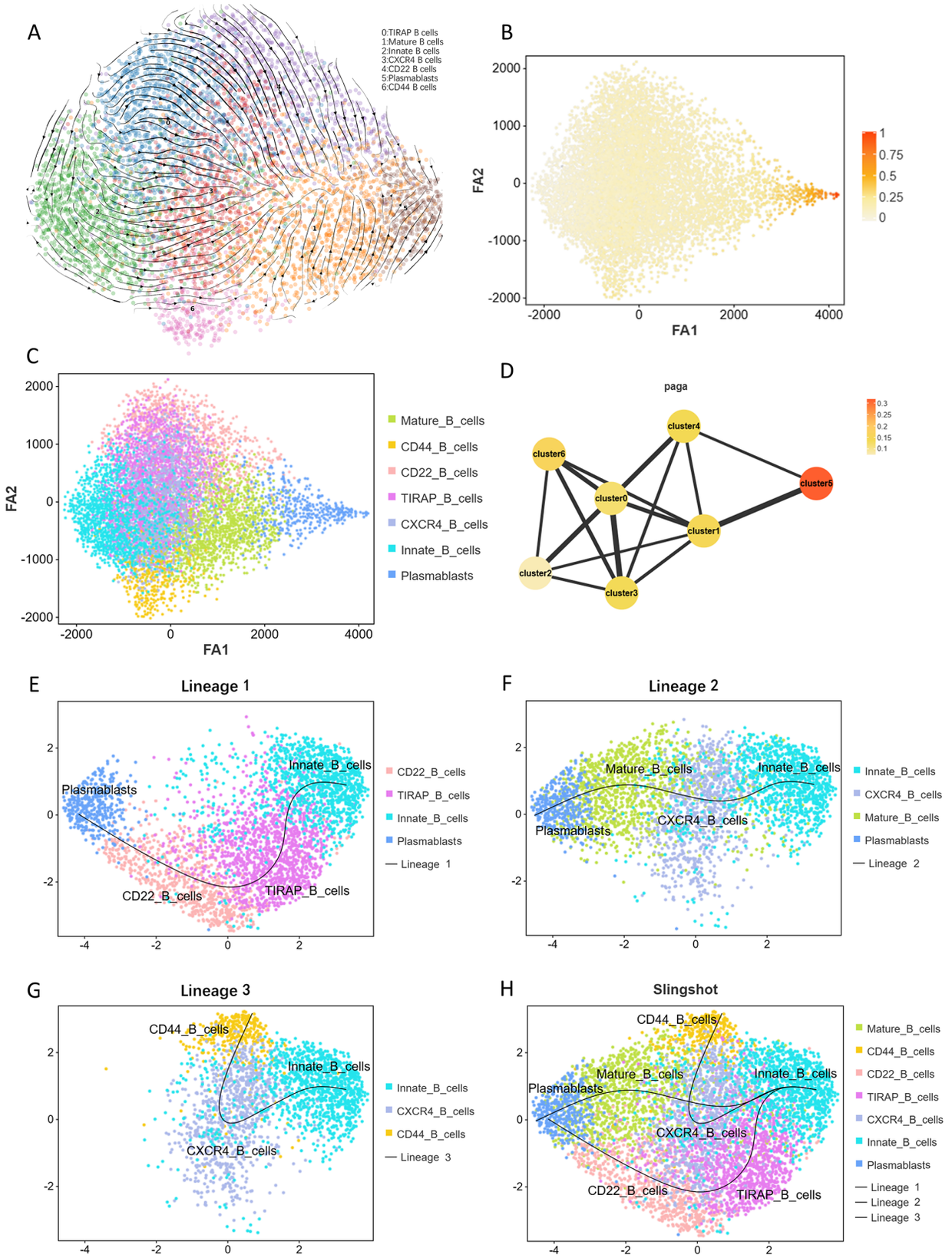

Figure 2 Single-cell pseudotime trajectory analysis of IgM$^+$ B cell subsets

A: RNA velocity analysis of IgM$^+$ B cell subsets, with velocity vectors projected onto the Seurat-generated UMAP embedding. B: PAGA scatter plot showing pseudotime progression of IgM$^+$ B cells, with color intensity indicating developmental state. C: PAGA scatter plot showing IgM$^+$ B cell subset identity, with colors denoting distinct subsets. D: Simplified PAGA topology graph showing hierarchical relationships among IgM$^+$ B cell subsets, with each node representing a subset, node color intensity indicating pseudotime progression, and edge thickness reflecting transcriptional similarity between subsets. E–G: Slingshot-inferred subsets contributing to lineage 1 (E), lineage 2 (F), and lineage 3 (G), with colors denoting distinct subsets. H: Summary of the three Slingshot-inferred lineages, with lines representing differentiation trajectories from a common root and colors denoting IgM$^+$ B cell subsets.

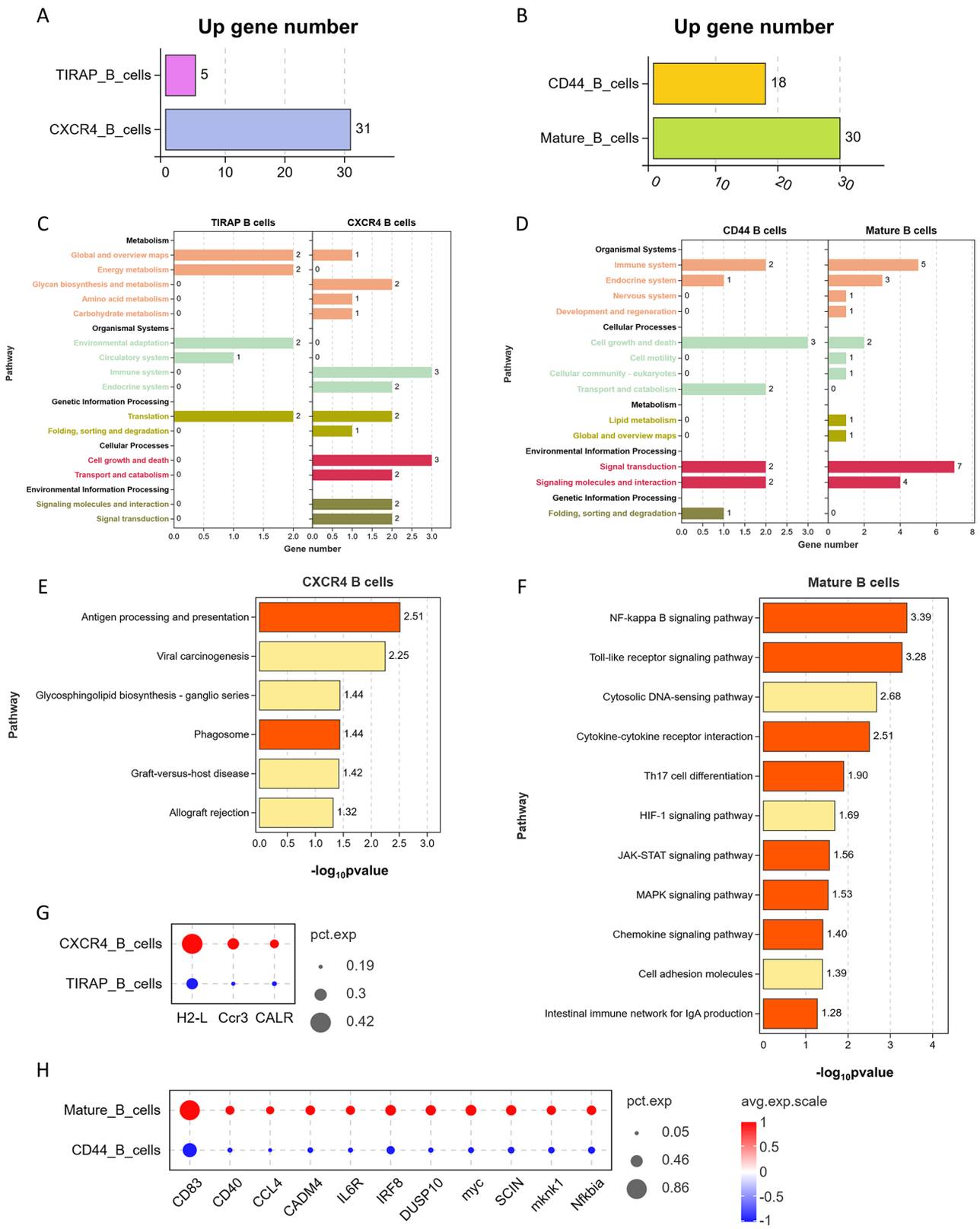

Figure 3 Differential gene expression between TIRAP$^+$ B cells and CXCR4$^+$ B cells and between mature B cells and CD44$^+$ B cells

A: Number of up-regulated genes in TIRAP$^+$ B cells and CXCR4$^+$ B cells. B: Number of up-regulated genes in mature B cells and CD44$^+$ B cells. C: GO enrichment of up-regulated genes in TIRAP$^+$ B cells and CXCR4$^+$ B cells across biological process (BP), molecular function (MF), and cellular component (CC) categories. D: GO enrichment of up-regulated genes in mature B cells and CD44$^+$ B cells across BP, MF, and CC categories. E: KEGG pathways enriched by up-regulated genes in CXCR4$^+$ B cells, with red bars indicating immune-related pathways. F: KEGG pathways enriched by up-regulated genes in mature B cells, with red bars indicating immune-related pathways. G: Bubble plot showing differential expression of key immune-related genes between TIRAP$^+$ B cells and CXCR4$^+$ B cells. H: Bubble plot showing differential expression of key immune-related genes between mature B cells and CD44$^+$ B cells.

pathways (Figure 3C), including antigen processing and presentation (ko04612) and phagosome (ko04145) pathways (Figure 3E). Genes associated with these enriched pathways included *H2-L*, *Ccr3*, and *CALR* (Figure 3G). Similarly, mature B cells displayed a higher number of up-regulated genes than $CD44^+$ B cells (Figure 3B), and were enriched in multiple immune regulatory pathways (Figure 3D), including the NF-κB signaling pathway (ko04064), Toll-like receptor signaling pathway (ko04620), cytokine-cytokine receptor interaction (ko04060), Th17 cell differentiation (ko04659), JAK-STAT signaling pathway (ko04630), MAPK signaling pathway (ko04010), chemokine signaling pathway (ko04062), and intestinal immune network for IgA production (ko04672) (Figure 3F). Pathway-associated genes in mature B cells included *CD83*, *CD40*, *CCL4*, *CADM4*, *IL6R*, *IRF8*, *DUSP10*, *myc*, *SCIN*, *mknk1*, and *Nfkbia* (Figure 3H).

Functional specialization of IgM^+ B cell subsets in phagocytosis and antigen presentation

Initial analysis of subset-enriched genes and associated pathways showed that cluster 2 (innate B cells) and cluster 5 (plasmablasts) contained the largest numbers of up-regulated genes (Supplementary Figure S5). Innate B cells also showed broad enrichment of pathways associated with innate immune activity. To further characterize the functional profile of this subset, GO and KEGG enrichment analyses were performed by comparing innate B cells with the remaining IgM^+ B cell clusters. In the GO Biological Process (BP) category, 15 leukocyte-related terms were selected from 187 significantly enriched terms (Figure 4B). These included receptor-mediated endocytosis (GO:0006898), lysosome organization (GO:0007040), positive regulation of granulocyte chemotaxis (GO:0071624), and regulation of granulocyte chemotaxis (GO:0071622), indicating strong involvement in innate immune processes (Figure 4E). KEGG enrichment analysis further identified pathways linked to innate immunity, including phagosome (ko04145), Fc gamma R-mediated phagocytosis (ko04666), antigen processing and presentation (ko04612), endocytosis (ko04144), and natural killer cell-mediated cytotoxicity (ko04650) (Figure 4C, D). To resolve the molecular network underlying the innate B cell phenotype, up-regulated genes in this subset were used to construct a PPI network in Cytoscape v.3.8.2 (Figure 4F). Representative genes associated with innate immune pathways identified by KEGG analysis were selectively highlighted to illustrate the molecular features of innate B cells (Figure 4A).

Functional specialization of IgM^+ B cell subsets in antibody secretion

Preliminary analysis of subset-enriched genes indicated that plasmablasts displayed transcriptional features associated predominantly with adaptive immunity. To further define this subset, GO and KEGG enrichment analyses were performed by comparing plasmablasts with the remaining IgM^+ B cell clusters. In the GO BP category, 15 immune-related terms, particularly those associated with adaptive immunity, were selected from 133 significantly enriched terms (Figure 5B). These terms included somatic recombination of immunoglobulin genes involved in immune response (GO:0002204), somatic diversification of immunoglobulins involved in immune response (GO:0002208), adaptive immune response (GO:0002250), immunoglobulin production (GO:0002377), immunoglobulin production involved in immunoglobulin-mediated immune response (GO:0002381), immunoglobulin-mediated immune response (GO:0016064), somatic diversification of immunoglobulins (GO:0016445), somatic recombination of immunoglobulin gene segments (GO:0016447), and B cell-mediated immunity (GO:0019724), highlighting strong enrichment of B cell and immunoglobulin-associated processes (Figure 5E). Consistent with these findings, KEGG analysis revealed enrichment of adaptive immune-related pathways, including intestinal immune network for IgA production (ko04672), B cell receptor signaling pathway (ko04662), and antigen processing and presentation (ko04612) (Figure 5C, D). To further resolve the molecular features of plasmablasts, up-regulated genes in this subset were used to construct a PPI network in Cytoscape v.3.8.2 (Figure 5F), and representative genes associated with adaptive immune pathways identified by KEGG analysis were selectively highlighted (Figure 5A). Based on the transcriptional profile and pathway enrichment of plasmablasts, a schematic model was generated to summarize the antibody-secretion program of IgM^+ B cells in the flounder head kidney (Figure 5G).

Enhanced BCR signaling and antigen presentation in vaccine-induced B cell responses

To investigate vaccine-associated transcriptional changes, integrated single-cell datasets were generated from the pVAA-injected vaccine group and pcDNA3.1-injected control group samples, followed by global differential expression analysis (Figure 6A). Compared with the control group, the vaccine group showed enrichment of multiple immune-related pathways, which were visualized using a circular enrichment plot. Among these pathways, B cell receptor (BCR) signaling was markedly up-regulated, and genes contributing to this pathway were highlighted in a schematic representation (Figure 6B). Comparative analysis of subset composition further showed that vaccination reduced the proportions of $TIRAP^+$ B cells and $CD22^+$ B cells, whereas the remaining subsets increased in relative abundance (Figure 6C, D). Notably, $TIRAP^+$ and $CD22^+$ B cells were located along lineage 1, whereas most subsets that expanded after vaccination were associated with lineage 2.

To characterize functional divergence among the three inferred trajectories, differential expression and pathway enrichment analyses were performed for two representative subset pairs: $TIRAP^+$ B cells versus $CXCR4^+$ B cells and mature B cells versus $CD44^+$ B cells. In the $TIRAP^+$ B cell and $CXCR4^+$ B cell comparison, 115 genes were up-regulated and 67 genes were down-regulated in $CXCR4^+$ B cells, whereas 85 genes were up-regulated and 35 genes were down-regulated in $TIRAP^+$ B cells (Supplementary Figure S6). KEGG enrichment analysis indicated that $CXCR4^+$ B cells in the vaccine group were more strongly associated with immune-related pathways, including Th17 cell differentiation (ko04659), intestinal immune network for IgA production (ko04672), Th1 and Th2 cell differentiation (ko04658), IL-17 signaling pathway (ko04657), B cell receptor signaling pathway (ko04662), and T cell receptor signaling pathway (ko04660) (Figure 6E, G).

In the mature B cell and $CD44^+$ B cell comparison, 75 genes were up-regulated and 36 genes were down-regulated in mature B cells, whereas 77 genes were up-regulated and 49 genes were down-regulated in $CD44^+$ B cells (Supplementary Figure S7). Despite the lower number of DEGs observed in mature B cells compared with $CD44^+$ B cells, KEGG pathway analysis revealed that mature B cells in the vaccine group were more functionally enriched in immune responses,

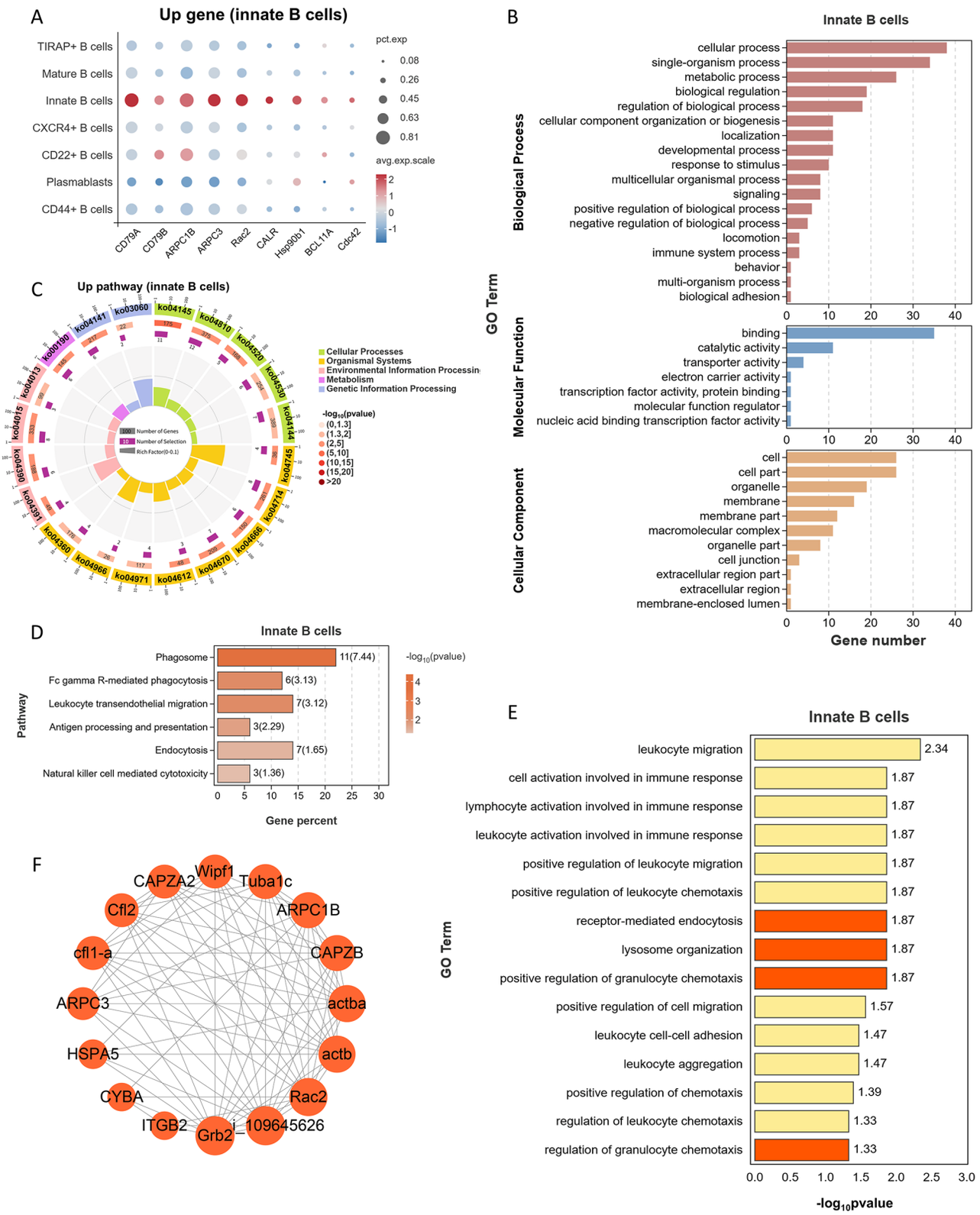

Figure 4 Functional characterization of innate B cell subset

A: Bubble plot showing expression of up-regulated genes in innate B cells. B: GO enrichment of up-regulated genes in innate B cells across biological process (BP), molecular function (MF), and cellular component (CC) categories. C: Enrichment circle plot showing top 20 KEGG pathways enriched by up-regulated genes in innate B cells. D: Six immune-related KEGG pathways enriched by up-regulated genes in innate B cells. E: Immune-related GO terms enriched by up-regulated genes in innate B cells, with red bars indicating terms associated with innate immunity. F: PPI network displaying key interactions among up-regulated genes in innate B cells.

including the T cell receptor signaling pathway (ko04660), Fc gamma R-mediated phagocytosis (ko04666), phagosome (ko04145), Th17 cell differentiation (ko04659), B cell receptor signaling pathway (ko04662), antigen processing and presentation (ko04612), and Th1 and Th2 cell differentiation (ko04658) (Figure 6F, H). Consistent with these functional features, both CXCR4^{+} B cells and mature B cells showed increased frequencies after vaccination and were positioned

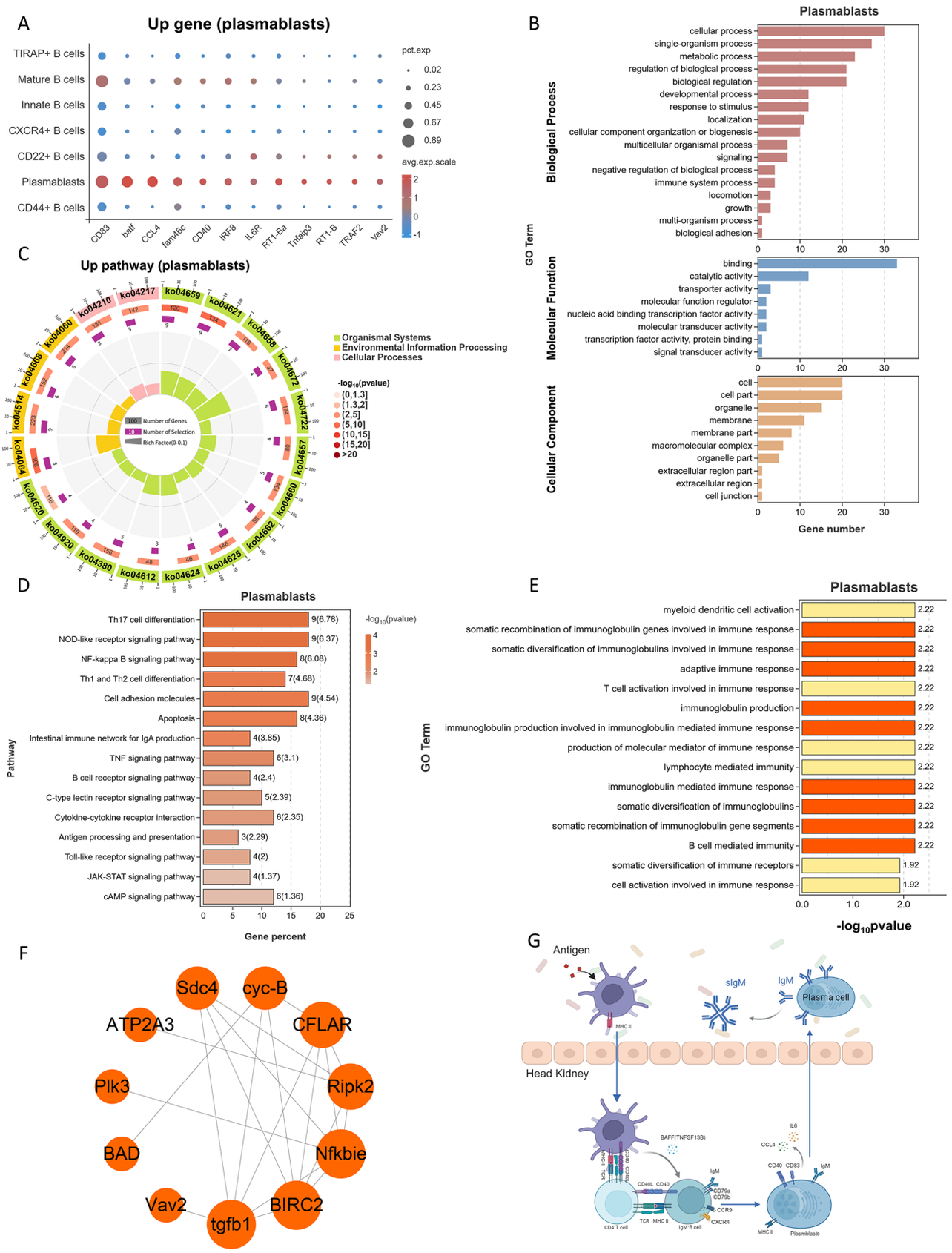

Figure 5 Functional characterization of plasmablasts subset

A: Bubble plot showing expression of up-regulated genes in plasmablasts. B: GO enrichment of up-regulated genes in plasmablasts across biological process (BP), molecular function (MF), and cellular component (CC) categories. C: Enrichment circle plot showing top 20 KEGG pathways enriched by up-regulated genes in plasmablasts. D: Fifteen immune-related KEGG pathways enriched by up-regulated genes in plasmablasts. E: Immune-related GO terms enriched by up-regulated genes in plasmablasts, with red bars indicating terms associated with immunoglobulin-related functions. F: PPI network showing key interactions among up-regulated genes in plasmablasts. G: Schematic model showing antibody secretion by IgM^+ B cells in the flounder head kidney.

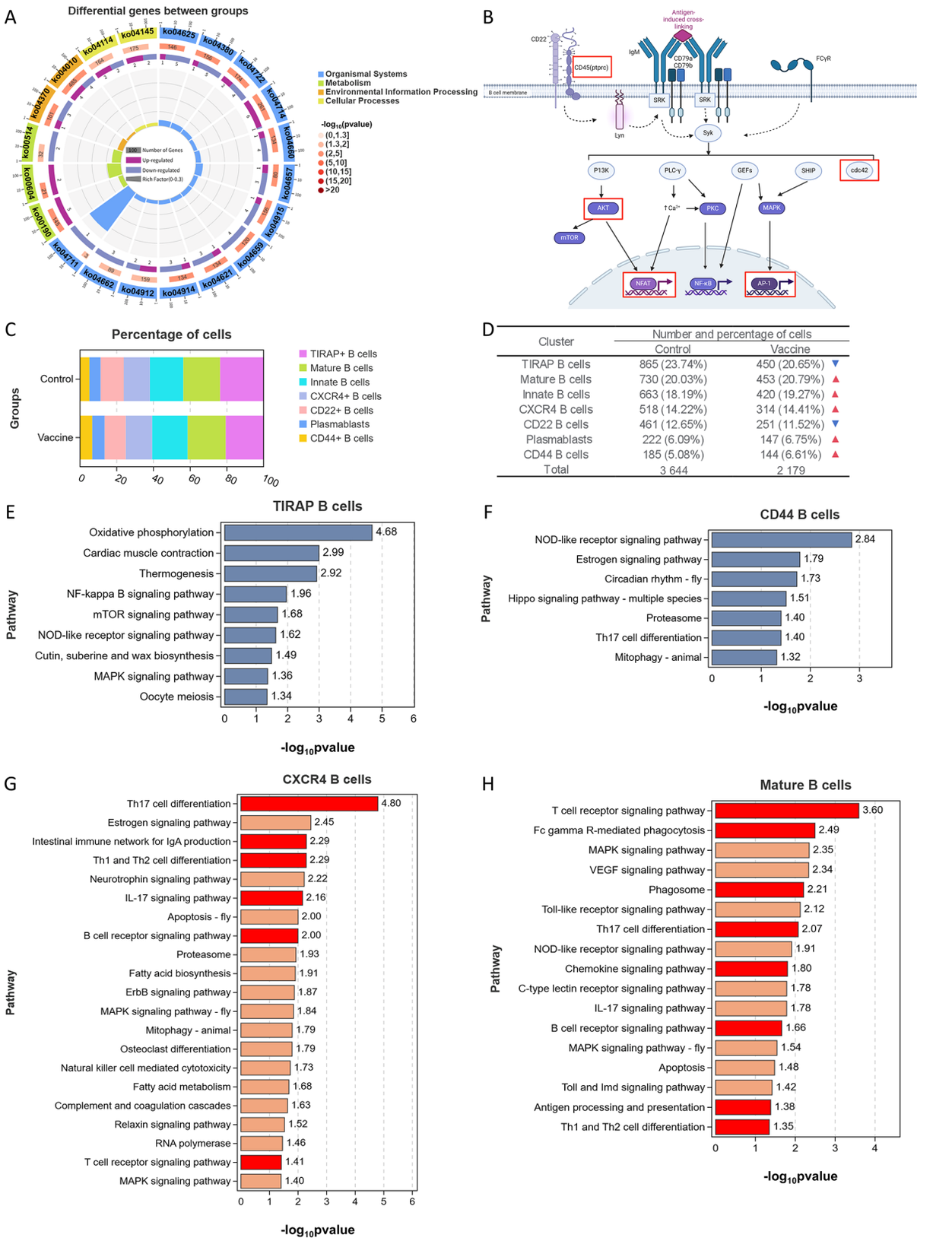

Figure 6 Comparative analysis of IgM$^+$ B cell subsets between control and vaccine groups

A: Enrichment circle plot showing top 20 KEGG pathways enriched by differentially expressed genes (DEGs) in IgM$^+$ B cells from the vaccine group compared to the control group. B: Schematic representation highlighting BCR signaling-related DEGs in IgM$^+$ B cells from the vaccine group (red boxes). C: Stacked bar chart showing percentage of each IgM$^+$ B cell subset in the control and vaccine groups. D: Absolute cell numbers and proportions of each IgM$^+$ B cell subset in the control and vaccine groups, with red arrows indicating subsets with increased proportions post-immunization and blue arrows indicating decreased proportions. E: KEGG pathway enrichment of DEGs in TIRAP$^+$ B cells. F: KEGG pathway enrichment of DEGs in CD44$^+$ B cells. G: KEGG pathway enrichment of DEGs in CXCR4$^+$ B cells. H: KEGG pathway enrichment of DEGs in mature B cells. Red bars indicate pathways related to T/B cell functions.

along lineage 2.

Based on the differentiation trajectories and immune functional characteristics of the seven IgM$^+$ B cell subsets, the top 10 immunization-induced DEGs were identified for each subset (Figure 7). Notably, vaccination preferentially enhanced transcriptional programs related to antigen presentation, BCR signaling, and cellular communication.

DISCUSSION

DNA vaccines confer durable protection by driving endogenous expression of pathogen-derived antigens and activating coordinated innate and adaptive immune responses (Liu, 2011). In teleosts, the protective efficacy of DNA vaccination has been demonstrated in multiple species, including rainbow trout (Ballesteros et al., 2015), Atlantic salmon (*Salmo salar*) (Houston et al., 2017), and flounder (Xing et al., 2019), with the DNA vaccine against salmon pancreas disease virus (SPDV) authorized for commercial use by the European Medicines Agency (Houston et al., 2017). IgM$^+$ B cells are major mediators of systemic immunity in teleosts and play central roles in vaccine-induced humoral responses (Rauta et al., 2012). Beyond antibody production,

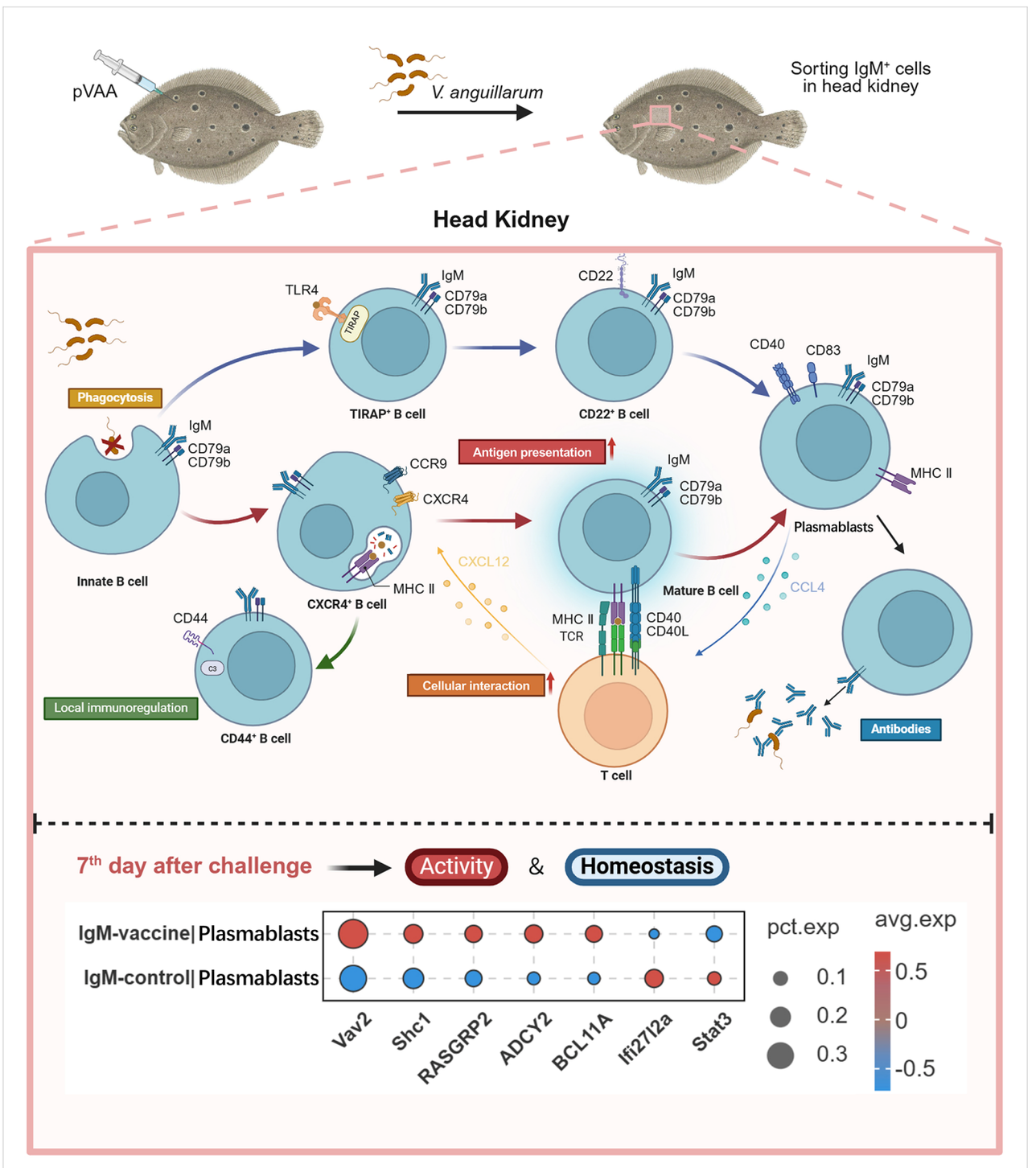

Figure 7 Proposed model of IgM$^+$ B cell-mediated protection in the flounder head kidney after vaccination and bacterial challenge, summarizing the protective roles of IgM$^+$ B cell subsets and immunization-induced gene expression changes across subsets

teleost IgM$^+$ B cells also exhibit marked phagocytic activity, a feature reported nearly two decades ago (Li et al., 2006). Recent scRNA-seq studies have further revealed substantial heterogeneity among teleost B cell populations, including those of rainbow trout (Perdiguero et al., 2021) and grass carp (*Ctenopharyngodon idella*) (Pan et al., 2023, 2025). Although IgM$^+$ B cells are widely recognized as principal effector cells after vaccination in teleosts, the subset-level programs through which these cells coordinate vaccine-induced protection remain insufficiently defined. In this study, IgM$^+$ B cells were sorted from flounder immunized with a *V. anguillarum* DNA vaccine and subsequently challenged with live bacteria, followed by scRNA-seq to resolve the cellular and transcriptional architecture of vaccine-responsive IgM$^+$ B cell subsets.

A multimodal trajectory-inference approach was employed to reconstruct differentiation trajectories among flounder IgM$^+$ B cell subsets. Initial pseudotime analysis with Monocle 2 provided limited resolution and did not clearly distinguish several subset transitions. This limitation may reflect subtle transcriptional differences among IgM$^+$ B cell subsets, as well as the sensitivity of Monocle 2 to incomplete reference genome annotation, which can reduce the accuracy of inferred differentiation trajectories (Qiu et al., 2017b). To improve trajectory reconstruction, RNA velocity, PAGA, and Slingshot were integrated as complementary analytical approaches. RNA velocity estimates the future direction of cell-state transitions from the relative abundance of unspliced and spliced mRNA, thereby addressing a key limitation of conventional pseudotime approaches, which often infer ordering without directional information (La Manno et al., 2018). PAGA provides a graph-based representation of topological connectivity among cell populations, enabling reconstruction of potential transition routes while reducing misclassification caused by distortion during dimensionality reduction (Wolf et al., 2019). Slingshot further infers lineage structure from predefined clusters and supports modeling of complex, multibranch differentiation programs (Street et al., 2018). Together, these approaches produced a more coherent and biologically plausible differentiation framework, providing a foundation for interpreting functional specialization among vaccine-responsive IgM$^+$ B cell subsets.

Three differentiation trajectories were identified among flounder IgM$^+$ B cells, each characterized by distinct molecular signatures and immune functional profiles. Lineage 1 exhibited features consistent with a T cell-independent (TI) B cell activation pathway. TIRAP$^+$ B cells showed high expression of *TIRAP* and *HMHA1* (RhoGAP45), suggesting rapid initiation of TLR-dependent signaling, with additional capacity to regulate cytoskeletal remodeling and immune-cell interactions during early infection (Ning et al., 2024; Trung et al., 2021). CD22$^+$ B cells were defined by *CD22* expression, a regulatory molecule involved in TLR signaling modulation and the maintenance and transition of BCR signaling responses (Clark & Giltiay, 2018). In contrast, lineage 2 displayed features more consistent with T cell-dependent (TD) activation. CXCR4$^+$ B cells expressed *CXCR4* and *CCR9*, suggesting pronounced chemotactic potential. Given the high expression of *CXCR4* in germinal center centroblasts, this subset may contribute to T cell-associated immune coordination in teleost B cell responses (Caron et al., 2009). Mature B cells exhibited transcriptional similarity to plasmablasts and high expression of macrophage-expressed gene 1 (*mpeg1*), suggesting a close functional relationship with macrophages and potential direct bactericidal capacity (Ferrero et al., 2020). In the vaccine group, *CD74*, *TNFSF13B*, and *CORO1C* were differentially expressed in CXCR4$^+$ B cells and mature B cells compared with TIRAP$^+$ B cells and CD44$^+$ B cells, and these genes were significantly enriched in T cell-related pathways (Figure 6E–H). Lineage 3 may represent a pathway associated with local immune regulation. CD44$^+$ B cells up-regulated *CD44*, *ATF4*, and *MYCBP*, indicating an activated state and enhanced adhesion and migration capacity (Cao et al., 2022b). Concurrent *C3* expression further suggested a role in local antigen clearance and regulation of the immune microenvironment (Wu et al., 2020). Collectively, these trajectories indicate that flounder IgM$^+$ B cells span a broad functional continuum, extending from innate immune initiation and T cell-associated activation to antibody secretion and tissue-directed migration. This developmental plasticity and functional integration differ from the more compartmentalized and specialized B cell subsets of mammals, suggesting that teleost B cell immunity exhibits less strict partitioning between innate and adaptive immune functions (Allman & Pillai, 2008). Such functional integration may enable teleosts to respond to diverse pathogen challenges despite the absence of canonical germinal centers and mammalian-type immunoglobulin class-switch recombination.

Seven transcriptionally distinct flounder IgM$^+$ B cell subsets were identified in this study. Drawing on previous studies of *V. anguillarum* infection and IgM$^+$ B cell responses in flounder, subsets 1, 2, and 5 were annotated as mature B cells, innate B cells, and plasmablasts, respectively (Hao et al., 2024; Li et al., 2007; Sheng et al., 2019; Xing et al., 2018). Similar B cell subsets with phagocytic, antigen-presenting, and antibody-secreting functions have also been reported in other teleost species, including rainbow trout and grass carp (Pan et al., 2023; Perdiguero et al., 2021). The remaining subsets were designated according to the relative enrichment of characteristic marker genes and were annotated as TIRAP$^+$ B cells, CXCR4$^+$ B cells, CD22$^+$ B cells, and CD44$^+$ B cells. Pseudotime analysis further suggested that these subsets contribute to sequential stages of IgM$^+$ B cell differentiation in flounder. However, the broad transcriptional divergence revealed by scRNA-seq requires subset-level biological validation. Future studies integrating functional assays with *in vivo* infection models will be necessary to elucidate the precise immunological roles of these populations.

Innate B cells appeared to occupy an early position in the inferred differentiation hierarchy. Expression of *CD79a/CD79b* (*Igα/Igβ*), which mediates early B cell activation (Dal Porto et al., 2004), together with *IL-5R* (Nishiya et al., 2020) and *TNFSF13B* (*BAFF*) (Tafalla et al., 2017), which support B cell viability, suggested that this subset represents an early-response B cell population with rapid differentiation capacity. Consistent with this interpretation, innate B cells were enriched in phagocytosis-related pathways, including Fc receptor-mediated phagocytosis (Hao et al., 2024). In addition, Blimp, encoded by *PRDM1*, was initially identified as a transcription factor rapidly induced during B cell differentiation into immunoglobulin-secreting cells (Turner et al., 1994), with more recent studies indicating an important role in innate immune cells, particularly myeloid cells (Nadeau & Martins, 2022; Severa et al., 2014). In the present study, Blimp was highly expressed in both innate B cells and mature B cells, consistent with findings in vaccinated flounder infected with *Edwardsiella tarda* (Wu et al., 2022b). These results suggest that flounder IgM$^+$ B cells combine antibody-related

differentiation capacity with transcriptional features associated with myeloid-like innate immune functions.

The high co-expression of *MHC II*, *CD83*, *CD40*, and *B7/CD80* in plasmablasts indicated that this subset retained antigen-presenting capacity and provided co-stimulatory signals required for T cell activation and downstream immune responses (Perdiguero et al., 2021; Xing et al., 2018). Expression of *CCL4* may strengthen intercellular communication by recruiting and activating immune cells, including T cells, thereby supporting formation of a coordinated local immune network (Xu et al., 2020). *IRF4* and *IRF8* regulate the differentiation of B cells into antibody-secreting cells by modulating transcriptional programs and cell fate decisions (Perdiguero et al., 2021). *mTOR* may coordinate these processes by integrating nutrient availability, metabolic status, and immune signaling, allowing plasmablasts to sustain effector functions under conditions of high biosynthetic demand (Cao et al., 2022a). The plasmablasts identified in flounder also retained antigen-presenting and phagocytic features, consistent with related IgM^+ B cell subsets reported in zebrafish (*Danio rerio*), Chinese tongue sole (*Cynoglossus semilaevis*), rainbow trout, and grass carp (Han et al., 2024; Wang et al., 2024; Wu et al., 2022a). These functional features resemble teleost macrophage functions and further suggest a close functional relationship between B cells and macrophage-like innate immune programs in teleost fish.

Activation of BCR signaling appeared to contribute to resistance against *V. anguillarum* infection, as BCR pathway-related DEGs, including *ptprc*, *cdc42*, *AKT*, *NFAT*, and *AP-1*, were significantly enriched in the vaccine group (Figure 6B). In mammals, *ptprc* encodes CD45, a key regulator of lymphocyte activation thresholds, and its increased expression in flounder suggests enhanced BCR pathway activity after vaccination (Huntington et al., 2006). Subset-level comparison further revealed that all four IgM^+ B cell subsets within lineage 2 increased in abundance and exhibited up-regulation of pathways associated with T/B cell interactions after vaccination (Figure 7). In innate B cells, up-regulation of *ptprc*, *fam46c*, and *PRKCB* was associated with BCR signaling and cytoskeletal remodeling, suggesting broad activation of this subset during the early immune response to infection (Al Barashdi et al., 2021; Tsui et al., 2018; Zhu et al., 2017). In $CXCR4^+$ B cells, elevated *GRB2* expression may link receptor-proximal signals, including BCR and CD40 pathways, to downstream MAPK activation, thereby strengthening co-stimulatory signal integration and promoting interactions with T cells (Ackermann et al., 2011). In mature B cells, increased expression of the MHC II invariant chain (*Ii*/*CD74*) and other antigen-presentation-associated components may improve antigen-presentation efficiency and promote T cell activation (Dijkstra & Yamaguchi, 2019).

IgM^+ B cells were collected at 7 days post-challenge, a time point at which no vaccinated flounder had died, indicating that pVAA immunization had conferred effective protection (Xing et al., 2019). Therefore, transcriptional profiling at this stage provided an opportunity to infer how IgM^+ B cell subsets contributed to protective immunity after bacterial challenge. This protective state was reflected most clearly in plasmablasts. The up-regulated genes *VAV2*, *Shc1*, *RasGRP2*, and *ADCY2* encode signaling regulators that integrate pathways controlling cell migration, proliferation, and antibody-secretion capacity, including small GTPases, MAPK, and cAMP signaling (Halls & Cooper, 2011; Luzi et al., 2000; Malhotra et al., 2009; Stone, 2006). *BCL11a* inhibits B cell apoptosis in mammals (Yu et al., 2012), and *BCL11a* expression in flounder B cells has been shown to limit hirame rhabdovirus (HIRRV) infection (Tang et al., 2022). Up-regulation of *VAV2*, *Shc1*, *RasGRP2*, *ADCY2*, and *BCL11a* in plasmablasts suggested that this subset retained antibody-producing potential and survival capacity during the protected post-challenge phase. In contrast, *Ifi27l2a*, an interferon-stimulated gene commonly induced during acute bacterial infection (Tantawy et al., 2014), and *STAT3*, a key mediator of JAK/STAT3-dependent IgM^+ B cell activation (Wu et al., 2025), were down-regulated. These transcriptional changes likely reflect attenuation of inflammatory signaling and progressive restoration of immune homeostasis. Thus, plasmablasts at 7 days post-challenge appeared to maintain effector capacity while shifting away from acute immune activation, a state that may support sustained pathogen control after effective vaccine-mediated protection.However, this interpretation remains inferential and requires systematic validation in future studies.

Overall, this study established a *V. anguillarum* challenge model after DNA vaccination in flounder and resolved head kidney IgM^+ B cell responses at single-cell resolution. After bacterial infection, IgM^+ B cells exhibited a coordinated differentiation framework spanning innate immune initiation, T cell-associated activation, antibody secretion, and tissue-directed migration across three developmental trajectories, highlighting the functional diversity of teleost B cells and the less compartmentalized organization of teleost B cell immunity compared with mammalian systems. Vaccination significantly enhanced BCR signaling, T/B cell interaction pathways, and antigen-processing programs. Plasmablasts showed a particularly dynamic transcriptional shift from active immune response toward immune homeostasis, suggesting that this subset may contribute to durable protection during the later stage of infection. Future studies should test the functional impact of T/B cell interactions on B cell-mediated protection through T/B cell co-culture systems and complementary immune assays. Integrated protein-level analyses and parallel profiling of additional immune populations, including T cells, will further define the cellular interaction network underlying vaccine-induced protection in flounder. Collectively, this study provides new insight into the cellular mechanisms through which teleost B cells support vaccine-mediated immune defense.

DATA AVAILABILITY

The sequencing raw data were deposited in the Sequence Read Archive (SRA) under accession number PRJNA1157710, Genome Sequence Archive (GSA) (https://ngdc.cncb.ac.cn/gsa/) under CRA043287, and Science Data Bank (DOI:10.57760/sciencedb.j00139.00312).

SUPPLEMENTARY DATA

Supplementary data to this article can be found online.

COMPETING INTERESTS

The authors declare that they have no competing interests.

AUTHORS' CONTRIBUTIONS

Z.J.M.: Writing–original draft, Validation, Investigation, Data curation. H.F.T.: Investigation, Data curation. J.X.: Writing–review & editing, Funding acquisition, Data curation, Conceptualization. X.Q.T.: Supervision, Methodology. X.Z.S.: Supervision, Methodology. H.C.: Supervision, Methodology. W.B.Z.: Supervision, Methodology. All authors read and approved the final version of the manuscript.

ACKNOWLEDGMENTS

We are grateful to Gene Denovo Biotechnology Co., Ltd. (Guangzhou, China) for assistance with sequencing and bioinformatics analysis.

REFERENCES

Ackermann JA, Radtke D, Maurberger A, et al. 2011. Grb2 regulates B-cell maturation, B-cell memory responses and inhibits B-cell Ca^{2+} signalling. *The EMBO Journal*, **30**(8): 1621–1633.

Al Barashdi MA, Ali A, Mcmullin MF, et al. 2021. Protein tyrosine phosphatase receptor type C (PTPRC or CD45). *Journal of Clinical Pathology*, **74**(9): 548–552.

Allman D, Pillai S. 2008. Peripheral B cell subsets. *Current Opinion in Immunology*, **20**(2): 149–157.

Ashburner M, Ball CA, Blake JA, et al. 2000. Gene ontology: tool for the unification of biology. *Nature Genetics*, **25**(1): 25–29.

Ballesteros NA, Alonso M, Saint-Jean SR, et al. 2015. An oral DNA vaccine against infectious haematopoietic necrosis virus (IHNV) encapsulated in alginate microspheres induces dose-dependent immune responses and significant protection in rainbow trout (*Oncorrhynchus mykiss*). *Fish & Shellfish Immunology*, **45**(2): 877–888.

Becht E, Mcinnes L, Healy J, et al. 2019. Dimensionality reduction for visualizing single-cell data using UMAP. *Nature Biotechnology*, **37**(1): 38–44.

Boshra H, Wang TH, Hove-Madsen L, et al. 2005. Characterization of a C3a receptor in rainbow trout and *Xenopus*: the first identification of C3a receptors in nonmammalian species. *The Journal of Immunology*, **175**(4): 2427–2437.

Bromage ES, Kaattari IM, Zwollo P, et al. 2004. Plasmablast and plasma cell production and distribution in trout immune tissues. *The Journal of Immunology*, **173**(12): 7317–7323.

Camp JG, Sekine K, Gerber T, et al. 2017. Multilineage communication regulates human liver bud development from pluripotency. *Nature*, **546**(7659): 533–538.

Cao JF, Ding LG, Wang QC, et al. 2022a. Conserved role of mTORC1 signaling in B cell immunity in teleost fish. *The Journal of Immunology*, **209**(6): 1095–1107.

Cao L, Fang H, Yan D, et al. 2022b. CD44a functions as a regulator of p53 signaling, apoptosis and autophagy in the antibacterial immune response. *Communications Biology*, **5**(1): 889.

Caron G, Le Gallou S, Lamy T, et al. 2009. CXCR4 expression functionally discriminates centroblasts versus centrocytes within human germinal center B cells. *The Journal of Immunology*, **182**(12): 7595–7602.

Chan JTH, Kadri S, Köllner B, et al. 2022. RNA-Seq of single fish cells - seeking out the leukocytes mediating immunity in teleost fishes. *Frontiers in Immunology*, **13**: 798712.

Clark EA, Giltiay NV. 2018. CD22: a regulator of innate and adaptive B cell responses and autoimmunity. *Frontiers in Immunology*, **9**: 2235.

Dal Porto JM, Gauld SB, Merrell KT, et al. 2004. B cell antigen receptor signaling 101. *Molecular Immunology*, **41**(6-7): 599–613.

Dijkstra JM, Yamaguchi T. 2019. Ancient features of the MHC class II presentation pathway, and a model for the possible origin of MHC molecules. *Immunogenetics*, **71**(3): 233–249.

Dornburg A, Yoder JA. 2022. On the relationship between extant innate immune receptors and the evolutionary origins of jawed vertebrate adaptive immunity. *Immunogenetics*, **74**(1): 111–128.

Fänge R. 1986. Lymphoid organs in sturgeons (*Acipenseridae*). *Veterinary Immunology and Immunopathology*, **12**(1-4): 153–161.

Ferrero G, Gomez E, Lyer S, et al. 2020. The *macrophage-expressed gene* (*mpeg*) *1* identifies a subpopulation of B cells in the adult zebrafish. *Journal of Leukocyte Biology*, **107**(3): 431–443.

Halls ML, Cooper DMF. 2011. Regulation by Ca^{2+}-signaling pathways of adenylyl cyclases. *Cold Spring Harbor Perspectives in Biology*, **3**(1): a004143.

Han XQ, Cui ZW, Ma ZY, et al. 2024. Phagocytic plasma cells in teleost fish provide insights into the origin and evolution of B cells in vertebrates. *The Journal of Immunology*, **213**(5): 730–742.

Hao YB, Xing J, Sheng XZ, et al. 2024. The role of Fc receptors in the innate immune system of flounders purported to be homologs of FcγRII and FcγRIII. *The Journal of Immunology*, **212**(7): 1196–1206.

Houston R, Moxon S, Nogué F, et al. 2017. Assessment of the potential integration of the DNA plasmid vaccine CLYNAV into the salmon genome. *EFSA Journal*, **15**(1): e04689.

Huntington ND, Xu YK, Puthalakath H, et al. 2006. CD45 links the B cell receptor with cell survival and is required for the persistence of germinal centers. *Nature Immunology*, **7**(2): 190–198.

Kanehisa M, Goto S. 2000. KEGG: Kyoto encyclopedia of genes and genomes. *Nucleic Acids Research*, **28**(1): 27–30.

Korsunsky I, Millard N, Fan J, et al. 2019. Fast, sensitive and accurate integration of single-cell data with Harmony. *Nature Methods*, **16**(12): 1289–1296.

La Manno G, Soldatov R, Zeisel A, et al. 2018. RNA velocity of single cells. *Nature*, **560**(7719): 494–498.

Lapuente D, Winkler TH, Tenbusch M. 2024. B-cell and antibody responses to SARS-CoV-2: infection, vaccination, and hybrid immunity. *Cellular & Molecular Immunology*, **21**(2): 144–158.

Li J, Barreda DR, Zhang YA, et al. 2006. B lymphocytes from early vertebrates have potent phagocytic and microbicidal abilities. *Nature Immunology*, **7**(10): 1116–1124.

Li Q, Zhan WB, Xing J, et al. 2007. Production, characterisation and applicability of monoclonal antibodies to immunoglobulin of Japanese flounder (*Paralichthys olivaceus*). *Fish & Shellfish Immunology*, **23**(5): 982–990.

Liu MA. 2011. DNA vaccines: an historical perspective and view to the future. *Immunological Reviews*, **239**(1): 62–84.

Luzi L, Confalonieri S, Di Fiore PP, et al. 2000. Evolution of Shc functions from nematode to human. *Current Opinion in Genetics & Development*, **10**(6): 668–674.

Ma J, Bruce TJ, Jones EM, et al. 2019. A review of fish vaccine development strategies: conventional methods and modern biotechnological approaches. *Microorganisms*, **7**(11): 569.

Malhotra S, Kovats S, Zhang WG, et al. 2009. Vav and Rac activation in B cell antigen receptor endocytosis involves Vav recruitment to the adapter protein LAB. *Journal of Biological Chemistry*, **284**(52): 36202–36212.

Munang'andu HM, Evensen Ø. 2019. Correlates of protective immunity for fish vaccines. *Fish & Shellfish Immunology*, **85**: 132–140.

Nadeau S, Martins GA. 2022. Conserved and unique functions of Blimp1 in immune cells. *Frontiers in Immunology*, **12**: 805260.

Ning XH, Han B, Peng Y, et al. 2024. LncRNA pol-lnc78 as a ceRNA regulates antibacterial responses via suppression of pol-miR-n199-3p-mediated SARM down-regulation in *Paralichthys olivaceus*. *Zoological Research*, **45**(1): 25–35.

Nishiya K, Sawada M, Dijkstra JM, et al. 2020. A fish cytokine related to human IL-3, IL-5, and GM-CSF, induces development of eosinophil/basophil/mast-cell type (EBM) granulocytes. *Developmental & Comparative Immunology*, **108**: 103671.

Pan YR, Han XQ, Tian TT, et al. 2025. Single-cell atlas of grass carp (*Ctenopharyngodon idella*) peripheral blood IgM^+ B cells provides insights into B cell-mediated immune responses in teleost fish. *Zoological Research*, **46**(5): 953–966.

Pan YR, Wu CS, Zhong YQ, et al. 2023. An atlas of grass carp IgM^+ B cells in homeostasis and bacterial infection helps to reveal the unique heterogeneity of B cells in early vertebrates. *The Journal of Immunology*, **211**(6): 964–980.

Perdiguero P, Morel E, Tafalla C. 2021. Diversity of rainbow trout blood B

cells revealed by single cell RNA sequencing. *Biology*, **10**(6): 511.
Qiu XJ, Hill A, Packer J, et al. 2017a. Single-cell mRNA quantification and differential analysis with Census. *Nature Methods*, **14**(3): 309–315.
Qiu XJ, Mao Q, Tang Y, et al. 2017b. Reversed graph embedding resolves complex single-cell trajectories. *Nature Methods*, **14**(10): 979–982.
Rabinovitch M. 1995. Professional and non-professional phagocytes: an introduction. *Trends in Cell Biology*, **5**(3): 85–87.
Rathor GS, Swain B. 2024. Advancements in fish vaccination: current innovations and future horizons in aquaculture health management. *Applied Sciences*, **14**(13): 5672.
Rauta PR, Nayak B, Das S. 2012. Immune system and immune responses in fish and their role in comparative immunity study: a model for higher organisms. *Immunology Letters*, **148**(1): 23–33.
Satija R, Farrell JA, Gennert D, et al. 2015. Spatial reconstruction of single-cell gene expression data. *Nature Biotechnology*, **33**(5): 495–502.
Severa M, Islam SA, Waggoner SN, et al. 2014. The transcriptional repressor BLIMP1 curbs host defenses by suppressing expression of the chemokine CCL8. *The Journal of Immunology*, **192**(5): 2291–2304.
Sheng XZ, Chai BH, Wang ZF, et al. 2019. Polymeric immunoglobulin receptor and mucosal IgM responses elicited by immersion and injection vaccination with inactivated *Vibrio anguillarum* in flounder (*Paralichthys olivaceus*). *Aquaculture*, **505**: 1–11.
Shibasaki Y, Afanasyev S, Fernández-Montero A, et al. 2023. Cold-blooded vertebrates evolved organized germinal center–like structures. *Science Immunology*, **8**(90): eadf1627.
Soleto I, Morel E, Muñoz-Atienza E, et al. 2020. *Aeromonas salmonicida* activates rainbow trout IgM$^+$ B cells signalling through Toll like receptors. *Scientific Reports*, **10**(1): 16810.
Steinel NC, Bolnick DI. 2017. Melanomacrophage centers as a histological indicator of immune function in fish and other poikilotherms. *Frontiers in Immunology*, **8**: 827.
Stone JC. 2006. Regulation of Ras in lymphocytes: get a GRP. *Biochemical Society Transactions*, **34**(5): 858–861.
Street K, Risso D, Fletcher RB, et al. 2018. Slingshot: cell lineage and pseudotime inference for single-cell transcriptomics. *BMC Genomics*, **19**(1): 477.
Sun Y, Huang T, Hammarström L, et al. 2020. The immunoglobulins: new insights, implications, and applications. *Annual Review of Animal Biosciences*, **8**: 145–169.
Tafalla C, González L, Castro R, et al. 2017. B cell-activating factor regulates different aspects of B cell functionality and is produced by a subset of splenic B cells in teleost fish. *Frontiers in Immunology*, **8**: 295.
Tang XQ, Sun PY, Wang HX, et al. 2022. Zinc finger protein BCL11A contributes to the abortive infection of *Hirame novirhabdovirus* (HIRRV) in B lymphocytes of flounder (*Paralichthys olivaceus*). *Journal of Virology*, **96**(24): e01470–22.
Tang XQ, Zhou L, Zhan WB. 2008. Isolation and characterization of pathogenic *Listonella anguillarum* of diseased half-smooth tongue sole (*Cynoglossus semilaevis* Günther). *Journal of Ocean University of China*, **7**(3): 343–351.
Tantawy MA, Hatesuer B, Wilk E, et al. 2014. The interferon-induced gene *Ifi27l2a* is active in lung macrophages and lymphocytes after influenza a infection but deletion of *Ifi27l2a* in mice does not increase susceptibility to infection. *PLoS One*, **9**(9): e106392.
Tian HF, Xing J, Tang XQ, et al. 2021. Identification and characterization of a master transcription factor of Th1 Cells, T-bet, within flounder (*Paralichthys olivaceus*). *Frontiers in Immunology*, **12**: 704324.
Trung NB, Nan FH, Wang IJ, et al. 2021. Expression, signal transduction, and function analysis of TIRAP and TRIF in Nile tilapia (*Oreochromis niloticus*). *Developmental & Comparative Immunology*, **117**: 103991.
Tsui C, Martinez-Martin N, Gaya M, et al. 2018. Protein kinase C-β Dictates B cell fate by regulating mitochondrial remodeling, metabolic reprogramming, and heme biosynthesis. *Immunity*, **48**(6): 1144–1159. e5.
Turner CA, Mack DH, Davis MM. 1994. Blimp-1, a novel zinc finger-containing protein that can drive the maturation of B lymphocytes into immunoglobulin-secreting cells. *Cell*, **77**(2): 297–306.
Villani AC, Satija R, Reynolds G, et al. 2017. Single-cell RNA-seq reveals new types of human blood dendritic cells, monocytes, and progenitors. *Science*, **356**(6335): eaah4573.
Wang HY, Chen JY, Li YN, et al. 2024. Single-cell RNA sequencing illuminates the ontogeny, conservation and diversification of cartilaginous and bony fish lymphocytes. *Nature Communications*, **15**(1): 7627.
Wolf FA, Hamey FK, Plass M, et al. 2019. PAGA: graph abstraction reconciles clustering with trajectory inference through a topology preserving map of single cells. *Genome Biology*, **20**(1): 59.
Wu LT, Chai YW, Gao AL, et al. 2025. IL-21 signaling promotes IgM$^+$ B cell proliferation and antibody production via JAK/STAT3 and AKT pathways in early vertebrates. *Developmental & Comparative Immunology*, **164**: 105325.
Wu LT, Qin ZD, Liu HP, et al. 2020. Recent advances on phagocytic B cells in teleost fish. *Frontiers in Immunology*, **11**: 824.
Wu LT, Yang YJ, Gao AL, et al. 2022a. Teleost fish IgM$^+$ plasma-like cells possess IgM-secreting, phagocytic, and antigen-presenting capacities. *Frontiers in Immunology*, **13**: 1016974.
Wu XY, Xing J, Tang XQ, et al. 2022b. Splenic protection network revealed by transcriptome analysis in inactivated vaccine-immunized flounder (*Paralichthys olivaceus*) against *Edwardsiella tarda* infection. *Frontiers in Immunology*, **13**: 1058599.
Xing J, Tian HF, Wang L, et al. 2018. Characterization of CD40$^+$ leukocytes in flounder (*Paralichthys olivaceus*) and its response after Hirame novirhabdovirus infection and immunization. *Molecular Immunology*, **104**: 79–89.
Xing J, Xu HS, Tang XQ, et al. 2019. A DNA vaccine encoding the VAA gene of *Vibrio anguillarum* induces a protective immune response in flounder. *Frontiers in Immunology*, **10**: 499.
Xing J, Xu HS, Wang Y, et al. 2017. Identification of immunogenic proteins and evaluation of four recombinant proteins as potential vaccine antigens from *Vibrio anguillarum* in flounder (*Paralichthys olivaceus*). *Vaccine*, **35**(24): 3196–3203.
Xu HS, Xing J, Tang XQ, et al. 2020. The effects of CCL3, CCL4, CCL19 and CCL21 as molecular adjuvants on the immune response to VAA DNA vaccine in flounder (*Paralichthys olivaceus*). *Developmental & Comparative Immunology*, **103**: 103492.
Ye JM, Kaattari I, Kaattari S. 2011. Plasmablasts and plasma cells: reconsidering teleost immune system organization. *Developmental & Comparative Immunology*, **35**(12): 1273–1281.
Yu Y, Wang JX, Khaled W, et al. 2012. Bcl11a is essential for lymphoid development and negatively regulates p53. *Journal of Experimental Medicine*, **209**(13): 2467–2483.
Zhu YX, Shi CX, Bruins LA, et al. 2017. Loss of *FAM46C* promotes cell survival in myeloma. *Cancer Research*, **77**(16): 4317–4327.
Zwollo P, Cole S, Bromage E, et al. 2005. B cell heterogeneity in the teleost kidney: evidence for a maturation gradient from anterior to posterior kidney. *The Journal of Immunology*, **174**(11): 6608–6616.